Schaefer, Dominik; Achmus, Martin; Abdel-Rahman, Khalid

Effect of Sand Type on Capacity Degradation of Cyclic Axially Loaded Piles

Coastal Structures 2019 - Nils Goseberg, Torsten Schlurmann (eds) - © 2019 Bundesanstalt für Wasserbau
ISBN 978-3-939230-64-9 (Online) - DOI: 10.18451/978-3-939230-64-9_094

Effect of Sand Type on Capacity Degradation of Cyclic Axially Loaded Piles

D. Schäfer, M. Achmus & K. Abdel-Rahman
Institute for Geotechnical Engineering, Leibniz University of Hannover, Germany

Abstract: Cyclic axial loading of piles leads to a reduction of skin friction with increasing load cycle numbers and therefore to a capacity degradation. It is believed that the reduction of skin friction is induced by compaction of the soil in the vicinity of the pile due to the application of cyclic shear stress. For cyclic designs interaction diagrams derived from model and field tests worldwide exist. However, the data bases of such interaction diagrams (pile types, ground conditions) differ. It is to be expected that pile dimensions and ground conditions affect the amount of degradation. At the authors' institute, the "capacity degradation method" (CDM) was developed, which combines finite element modelling and cyclic direct simple shear (DSS) testing and allows the calculation of interaction diagrams accounting for the pile dimensions (considered in the numerical model) and soil type (investigated in the cyclic DSS tests). In this paper, results of DSS tests with three different sand soils, in which the volume compaction dependent on cyclic shear strain, relative density and initial normal stress was measured, are presented. These results are applied in CDM calculations in order to investigate the effect of sand type on the capacity degradation of piles.

Keywords: pile, cyclic axial loading, capacity degradation, direct simple shear test, sand

1 Introduction

Any kind of offshore installation, e.g. wind turbines or platforms, are loaded by wind and waves. The cyclic variation of these loads over its lifetime has to be considered in design proofs. Depending on the requirements and environmental conditions, different types of foundation structures are used. In many cases jacket or tripod structures supported by four or three piles are selected. These piles transfer the cyclic loads due to wind and waves to the subsoil mainly by axial forces, i.e. via skin friction and base resistance.

It is well known that piles under cyclic axial tensile and/or compressive loading exhibit considerable reductions of its bearing capacity with increasing number of load cycles (see e.g. Poulos, 1988, Jardine & Standing, 2012, Puech & Garnier, 2017). Derived from a multiplicity of field and model tests carried out worldwide several so-called interaction diagrams are available to assess the amount of capacity degradation. However, all interaction diagrams are valid for specific ground conditions and pile types and dimensions only. As an example, Fig. 1 shows the interaction diagram proposed by Jardine & Standing (2012) derived from field tests on driven steel pipe piles (diameter D = 0.46 m, embedded length L = 19 m) in dense quartz sand. Here, X_{cyc} and X_{mean} are the ratios of cyclic load amplitude and mean load, respectively, to the static pile capacity. With a given combination of cyclic and mean load, the number of cycles leading to pile failure can be read off the diagram. For other pile and ground conditions, different interaction diagrams apply (see for instance Poulos, 1988, Kirsch et al., 2011, Puech & Garnier, 2017). It is widely unclear how varying conditions affect the cyclic capacity degradation. In this paper, the focus lies on the effect of sand type on the degradation behaviour of piles under cyclic axial loading.

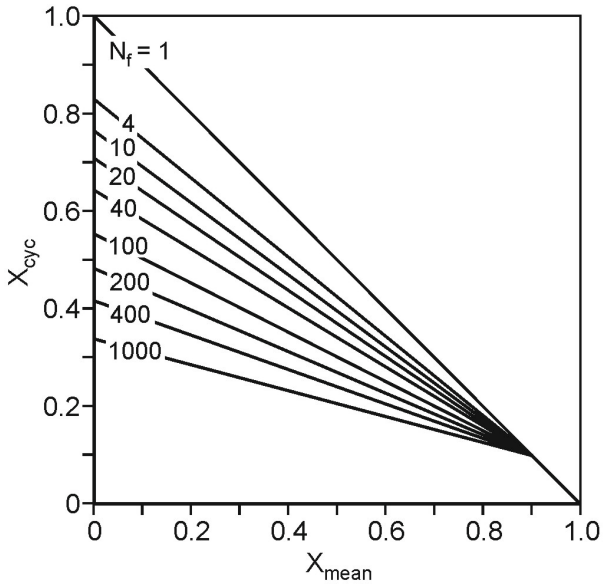

Fig. 1. Interaction diagram proposed by Jardine & Standing (2012).

It is assumed that the loss of skin friction capacity is the main reason for the observed degradation of pile capacity and that the reduction of skin friction is induced by compaction of the soil in the vicinity of the pile due to the application of cyclic shear stress.

For piles in sand, ultimate skin friction can be derived from the product of the normal stress acting on the pile shaft and the coefficient of friction, namely the tangent of the contact friction angle δ. The contact friction angle depends on the surface roughness of the pile shaft material and the type and relative density of the sand. It is usually assumed that the contact friction angle does not change significantly during cyclic pile loading. Hence, it must be expected that the normal stress acting on the pile shaft changes during cyclic loading. It is believed that the main reason for pile capacity degradation is the tendency of soil to contract under cyclic shear loading. In the vicinity of the pile shaft, this tendency to contractancy leads to a stress relaxation, i.e. to a reduction of the normal stress acting on the pile shaft.

Contractancy or compaction of soil under cyclic shearing can be observed in cyclic direct simple shear (DSS) tests under constant normal loading. The paper at hand presents the results of such tests. The behaviour of three sands with differing grain size distributions was investigated in series of cyclic DSS tests. The results were used as input to the CDM method (Achmus et al., 2015) in order to quantify the effect of sand type on the capacity degradation of cyclic axially loaded piles.

2 Experimental investigation

Comprehensive element tests in a direct simple shear apparatus were conducted to investigate the compaction behaviour of different sands due to shear loading under variation of several influencing values, namely initial relative density, effective normal stress, shear strain amplitude, number of cycles and cyclic load type. Similar tests with a medium to coarse grained uniform sand have been conducted by Silver & Seed (1971). These test results are used here for comparison.

2.1 DSS test device

Cyclic direct simple shear tests were selected for the element tests to analyse the compaction behaviour of the sandy soils. The specimen in the employed direct simple shear apparatus has a diameter of 70.4 mm and a height of 20.0 mm. It is placed inside approx. 20 teflon-coated, 1.0 mm thick confining rings of a very high radial stiffness and an intermediate latex membrane of approx. 300 µm thickness.

The previously homogenised sands were prepared in different relative densities by horizontal vibration and light vertical compression of an appropriate soil mass into the specimen volume. Subsequently, the entire simple shear box was carefully mounted into the apparatus, the upper load plate was manually driven downwards slightly before contact, the latex membrane was fixed to the

upper load plate and finally the automatic test procedure was started. The apparatus is shown in Fig. 2. All tests were performed strain-controlled under constant normal load (CNL) and sinusoidal alternating shear load at a frequency of 0.5 Hz over 10^3 load cycles. In a few tests, even 10^4 load cycles have been applied.

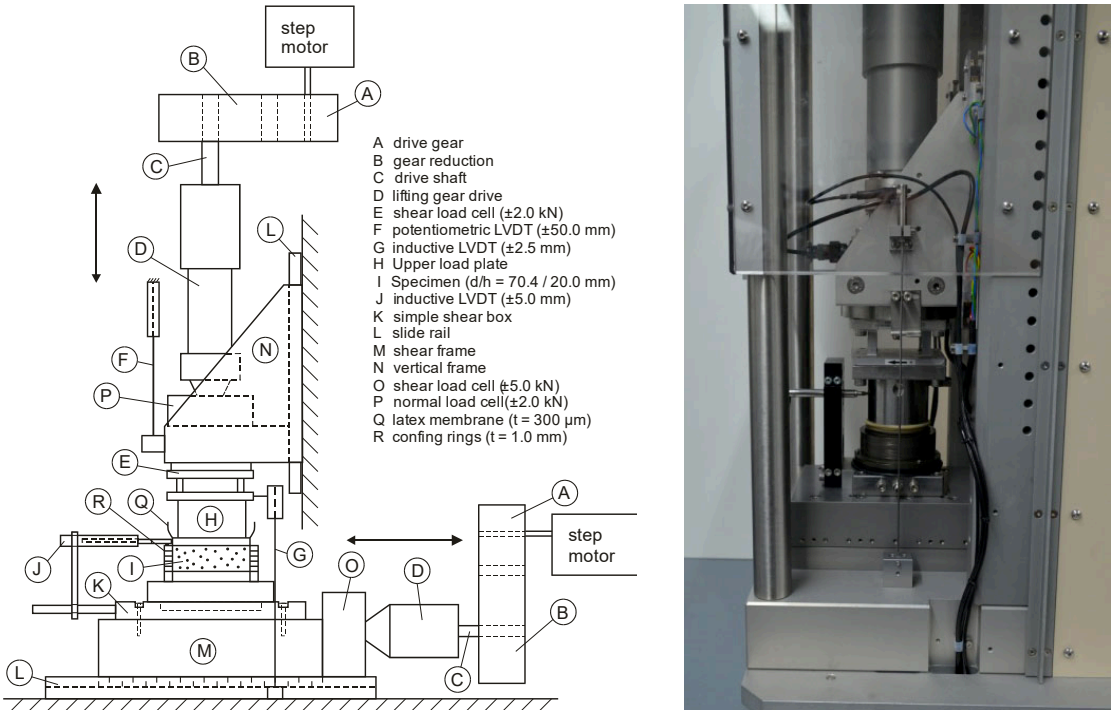

Fig. 2. Cyclic direct simple shear apparatus, sketch (left) and photography (right).

2.2 Scope of the parameter study

The parameter study was planned and executed in order to examine the individual effects of all mainly influencing values as follows:

- Grain size distributions: Three sands with differing grain size distributions were investigated (see Fig. 3, here also the sand used from Silver & Seed, 1971, is shown)
- Initial relative density: Samples were prepared to initial relative densities D_r of 0.5 / 0.75 (0.85 for Sand 2) / 1.0
- Effective normal stress: The normal stress acting on the sample was varied with σ = 100 / 200 / 400 / 600 kPa
- Cyclic shear strain span: The shear strain span $\Delta\gamma_{xy}$ is defined as the difference between maximum and minimum shear strains applied:

$$\Delta\gamma_{xy} = \gamma_{xy,max} - \gamma_{xy,min} \quad (1)$$

where $\gamma_{xy,min}$ = minimum cyclic shear strain, $\gamma_{xy,max}$ = maximum cyclic shear strain. Hence, the shear strain span used here is double of the shear strain amplitude. 6 shear strain spans were investigated: $\Delta\gamma_{xy} = 5.0\cdot10^{-4}$ / $1.0\cdot10^{-3}$ / $1.5\cdot10^{-3}$ / $2.0\cdot10^{-3}$ / $5.0\cdot10^{-3}$ / $1.0\cdot10^{-2}$

- Loading type / mean shear strain: In most of the tests, two-way loading with a mean shear strain $\gamma_{xy,mean}$ = 0 was applied. Only in tests with Sand 2, also the mean shear strain $\gamma_{xy,mean}$ was varied. The parameter R_m (see Fig. 4) is used to characterize the load type:

$$R_m = \frac{\gamma_{xy,mean}}{\gamma_{xy,max}} \quad (2)$$

where $\gamma_{xy,mean}$ = mean cyclic shear strain.

In all tests, 10^3 load cycles were applied at minimum. In sum, over 500 tests were performed.

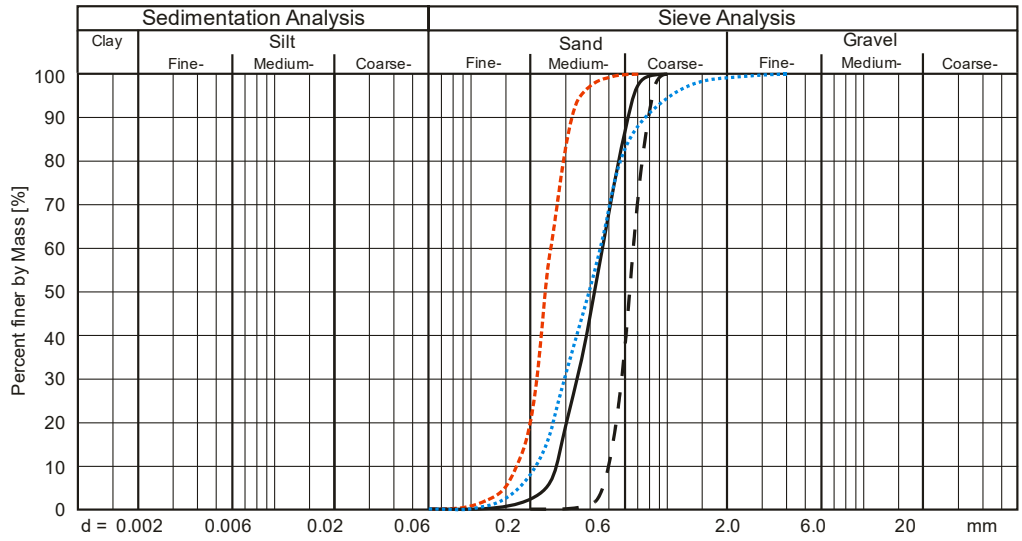

Line type				
Name	Sand 1	Sand 2	Sand 3	Silver&Seed
Soil type	fsaMSa	csaMSa	fsacsaMSa	fsaMSa
e_{min} / e_{max}	0.553 / 0.873	0.493 / 0.789	0.534 / 0.825	0.645 / 0.974
C_U / C_c	1.4 / 1.0	1.8 / 1.0	2.3 / 1.0	1.4 / 1.0

Fig. 3. Grain size distributions and extremal void ratios of the sands used.

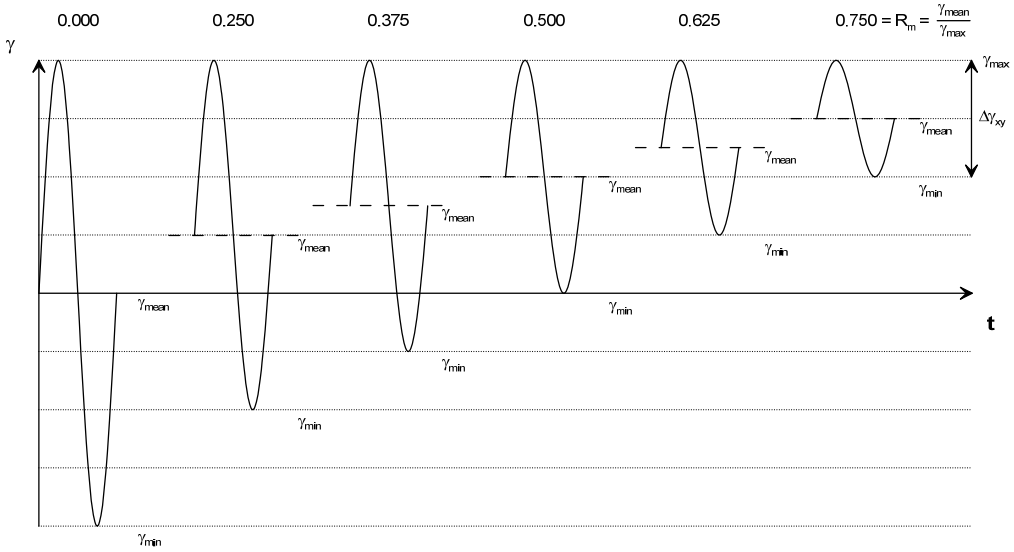

Fig. 4. Examined load types.

2.3 Results of the experimental investigation

2.3.1 General outcomes

In Figs. 5, 6 and 7 the general compaction behaviour of the three sands is presented in terms of the normal strains $\varepsilon_{N,c}$ dependent on the number of cycles N and the shear strain spans $\Delta\gamma_{xy}$ (these tests were conducted with $\gamma_{xy,mean} = 0$, i.e. $R_m = 0$, cf. Fig. 4). Only the results for $D_r = 0.5$ and 1.0 as well as $\sigma_N = 100$ and 600 kPa are presented. It is assumed that the reason for the partly discontinuous course of the curves, which occur more often at a high relative density and normal stress on the poorly-graded "Sand 1", is an intermittently stable packing state comparable with the stick-slip phenomenon of friction contacts.

Sand 1 is the finest material (medium sand with 20 % fine sand content). Sands 2 and 3 are both uniform medium sands with almost equal mean grain diameter, but Sand 3 has a higher content of both coarse sand and fine sand.

The compaction behaviour of Sand 1 and Sand 2 is nearly identical. On comparison, Sand 3 shows a tendency of slightly higher compaction.

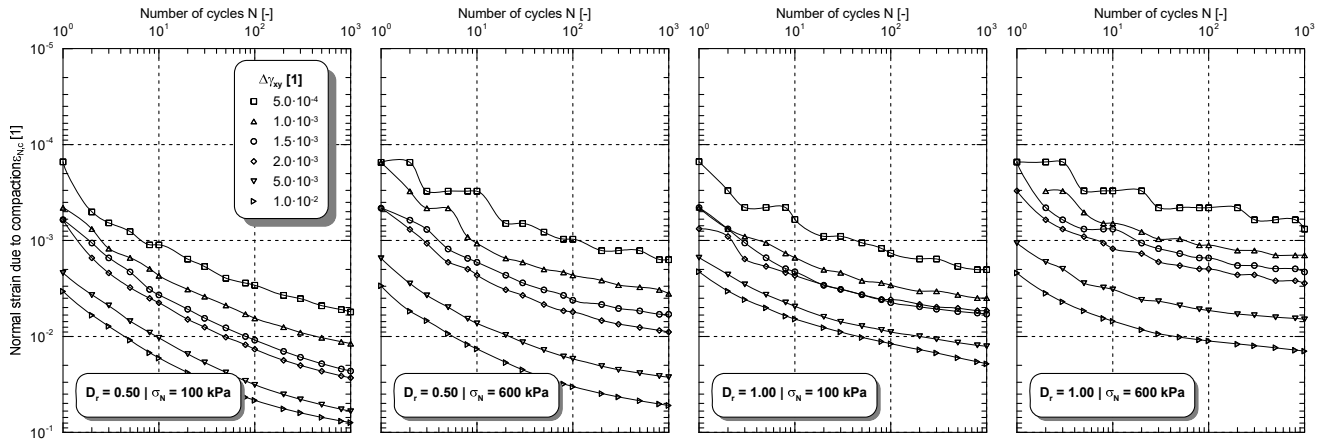

Fig. 5. Normal strain $\varepsilon_{N,c}$ over number of cycles N and shear strain span $\Delta\gamma_{xy}$ for "Sand 1" at an initial relative density of $D_r = 0.50$ and 1.00 and normal stresses $\sigma_N = 100$ kPa and 600 kPa.

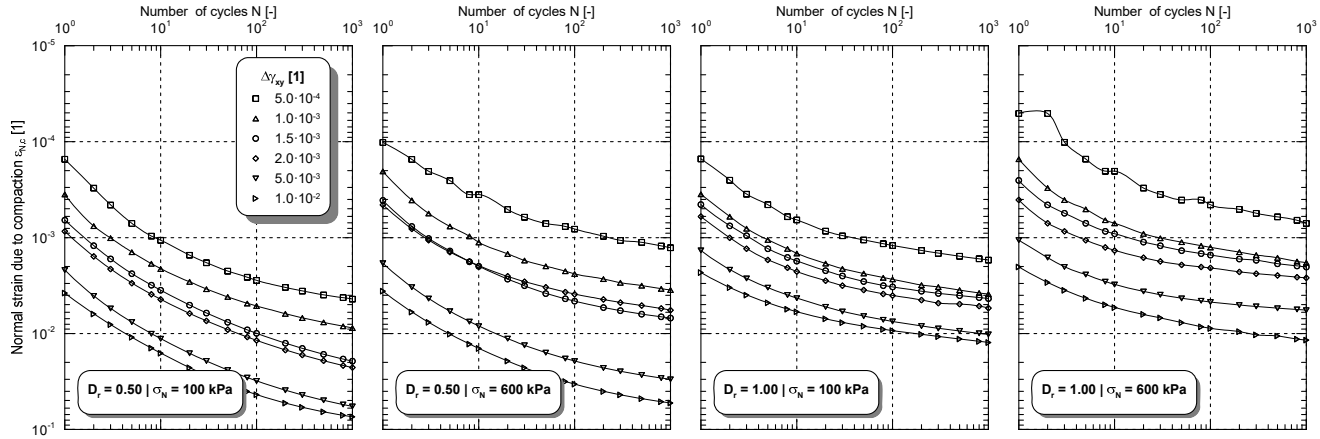

Fig. 6. Normal strain $\varepsilon_{N,c}$ over number of cycles N and shear strain span $\Delta\gamma_{xy}$ for "Sand 2" at an initial relative density of $D_r = 0.50$ and 1.00 and normal stresses $\sigma_N = 100$ kPa and 600 kPa.

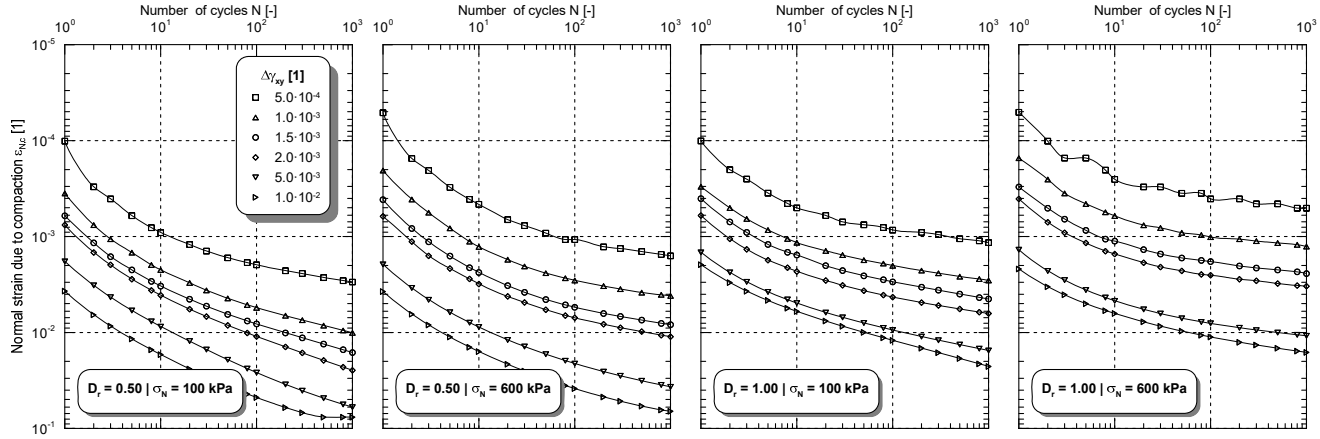

Fig. 7. Normal strain $\varepsilon_{N,c}$ over number of cycles N and shear strain span $\Delta\gamma_{xy}$ for "Sand 3" at an initial relative density of $D_r = 0.50$ and 1.00 and normal stresses $\sigma_N = 100$ kPa and 600 kPa.

The results indicate a negligible influence of the mean grain size. On the contrary, the course of the grain size distribution seems to affect the compaction behaviour, since the material with the greater uniformity index ("Sand 3") exhibits a slightly larger compaction in high normal stress states and denser packing.

2.3.2 *Load type influence*

The parameter study on "Sand 2" included an analysis of the influence of different load types, i.e. of mean shear strain, as elucidated in Fig. 4. For each load type, characterized by the parameter R_m, all other input values including the cyclic shear strain were varied. Fig. 8 presents the resulting normal strains for a relative density of 0.85 after 10 cycles under differing load types, maximum cyclic shear strains and normal stresses.

Evidently, identical cyclic shear strain spans with varying mean shear strains exhibit almost identical normal strains. This strongly indicates that the load type (initial displacement out off the starting position) influence is negligible. Therefore, in the tests with "Sand 1" and "Sand 3" the mean shear strain was set to zero (R_m=0) and no variation was made.

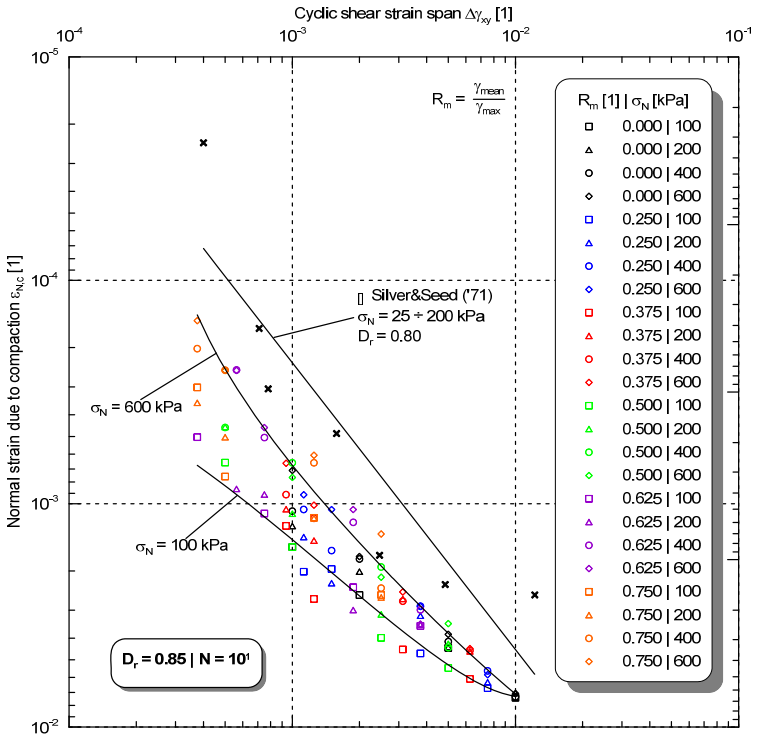

Fig. 8. Normal strain $\varepsilon_{N,c}$ over shear strain span $\Delta\gamma_{xy}$ for varying mean shear strains ("Sand 2").

2.3.3 *Effect of normal stress and relative density*

Supplemental to Fig. 6, also Fig. 8 illustrates the effect of normal stress on the compaction behaviour under cyclic shear strain for "Sand 2". Evidently, at higher stresses smaller volume contraction takes place. The effect seems to vanish at larger shear strains. It is assumed that a higher relative density as well as a higher normal stress state have a stabilising effect on the grain structure in such a manner that grain relative displacements or grain rearrangements are restrained and hence the soil exhibits a more elastic behaviour. Similar behaviour was observed for "Sand 1" and "Sand 3" as shown in Fig. 5 and Fig. 7.

2.3.4 *Summary of experimental results*

Fig. 9 compares results for the investigated sands exemplarily for a load cycle number of N = 10. Also the experimental results reported by Silver & Seed (1971) for a medium to coarse uniform sand (cf. Fig. 3) are given for comparison.

For each material investigated here, interpolation functions were developed which allow the determination of the volume compaction dependent on relative density, cyclic shear strain span, normal stress and number of load cycles. These functions were then used in numerical simulations with the CDM, as described in the next section. For calculations of number of cycles N>1000 extrapolations of the derived functions were used.

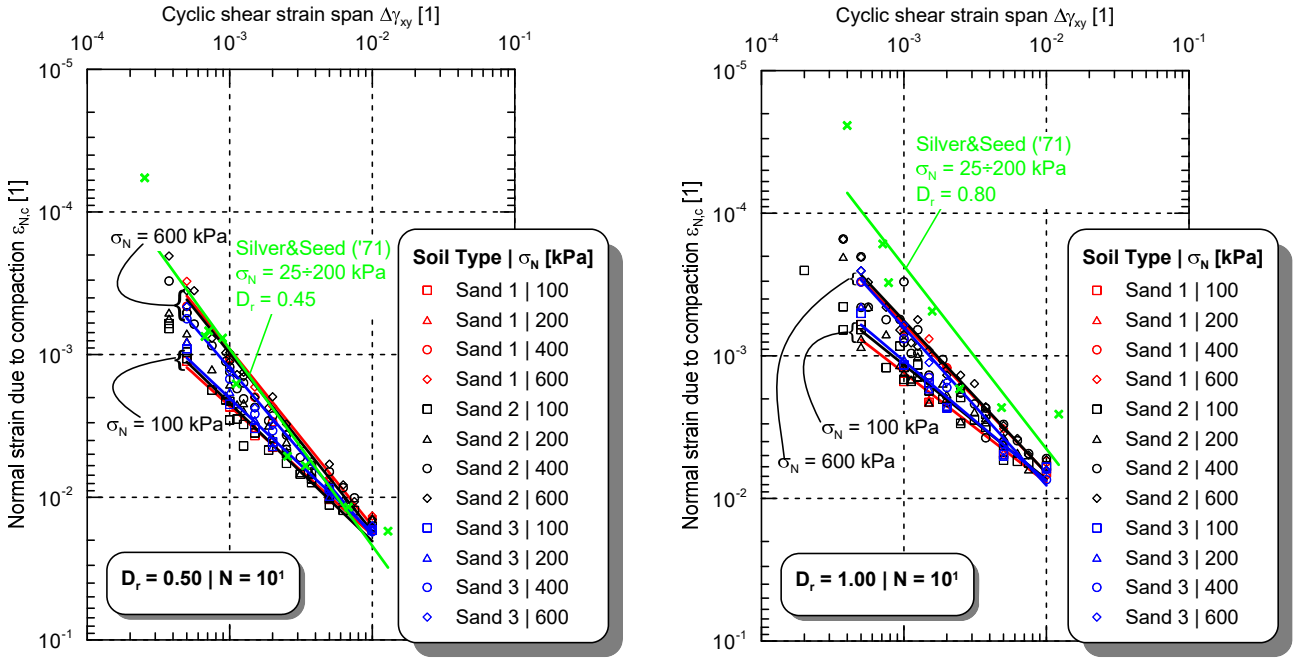

Fig. 9. Normal strain $\varepsilon_{N,c}$ over shear strain span $\Delta\gamma_{xy}$ at an initial relative density of 0.50 (left) and 1.00 (right) for the investigated sands with comparison to the results of Silver & Seed (1971).

3 Numerical simulation

3.1 General model description

The capacity degradation method applied here combines the finite element simulation of the pile with the surrounding soil under axial loading (2D axisymmetric model) with cyclic DSS tests characterizing the soil behaviour under cyclic loading. In the first step, a numerical pull-out test is conducted to determine the static pile capacity F_{ult}. In a following step, the pile in the numerical model is loaded to F_{max} and then unloaded to F_{min} (which yields the dimensionless load parameters $X_{mean} = 0.5\ (F_{max} + F_{min})/F_{ult}$ and $X_{cyc} = 0.5\ (F_{max} - F_{min})/F_{ult}$). This results in shear stresses $\gamma_{xy,max}$ and $\gamma_{xy,min}$ in the soil elements of the model and hence in a cyclic shear strain span $\Delta\gamma_{xy}$ for each element. Also the initial normal (radial) stress in each element is obtained. With these quantities, the volume compaction to be expected after a given number of load cycles can be determined from the results of cyclic DSS tests presented in the preceding section. In the 'small strain'-shear range soil behaves almost like an elastic material, and no volume compaction is to be expected, see e.g. Vucetic (1994). Therefore, if the shear strain amplitude $\gamma_{xy} = \Delta\gamma_{xy,i} / 2$ falls below a threshold strain γ_{lim}, $\varepsilon_{N,c}$ can be set to zero. The magnitude of the threshold strain is dependent on the soil type (Vucetic, 1994). In the investigation presented here, the threshold strain was assumed to be $\gamma_{lim} = 5 \cdot 10^{-5}$. In DSS tests not presented here, it could be confirmed that for strain amplitudes below this value, no measurable volume compaction occurred.

The determined volume compaction is then applied to the numerical model by "shrinking" the soil elements accordingly. The result is a stress redistribution and a decrease of the normal stresses acting on the pile shaft. A post-cyclic pull-out simulation finally yields the degraded pile capacity. By systematic variation of the number of load cycles, also the load cycle number N_f which leads to pile failure for a certain load combination F_{max} / F_{min} or X_{mean} / X_{cyc}, respectively, can be determined. This makes the derivation of an interaction diagram for the considered pile-soil system possible.

Details of the CDM can be found in Achmus et al. (2015) and Achmus et al. (2017). To account for the non-linear soil behaviour, elasto-plastic material behaviour was assumed for the soil elements. A Mohr-Coulomb failure criterion (parameters φ', c', ψ) was considered. A stress dependency of the oedometric stiffness modulus was implemented as follows:

$$E_s = \kappa \cdot \sigma_{atm} \cdot \left(\frac{\sigma_m}{\sigma_{atm}}\right)^{\lambda} \quad (3)$$

where σ_{atm} = 100 kPa = reference (atmospheric) stress, σ_m = current mean principal stress, κ = parameter for the stiffness at the reference stress state, λ = parameter for the stress dependency. The material parameters typical for medium dense sand used here are given in Table 1.

Tab. 1. Soil properties for medium dense sand used in the simulations.

Soil property	*Value*
Buoyant unit weight γ'	10.0 kN/m³
Oedometric stiffness parameter κ	600
Oedometric stiffness parameter λ	0.55
Poisson's ratio ν	0.25
Internal friction angle φ'	35.0°
Dilation angle ψ	5.0°
Cohesion c'	1.0 kN/m²

The numerical modelling was performed here for a steel tube pile with a length of 50 m, diameter of 2.0 m and a wall thickness of 3.0 cm. A linear elastic material behaviour of the pile was assumed with the parameters $E = 2.1 \cdot 10^5$ MPa (Young's modulus) and $\nu = 0.20$ (Poisson's ratio) for steel. For simplification, a homogeneous solid pile cross section was modelled. The elastic parameters were adapted to ensure axial pile stiffness equal to the stiffness of the steel tube. However, it should be noted that a change of the cyclic shear strain spans with increasing load cycle numbers, which is to be expected for long piles due to their limited axial stiffness, is not taken into account here. This would require updates of the shear strain spans during cyclic loading.

For the contact behaviour of the surface between pile and soil an elasto-plastic model was used. The maximum frictional shear stress is dependent on the normal stress σ_n and a coefficient of friction μ. In the numerical simulations presented here $\mu = \tan(2/3 \cdot \varphi') = 0.431$ was assumed. For full mobilisation of the limit frictional stress the relative displacement (elastic slip) between the pile and the surrounding soil was set to $\Delta u_{el,slip} = 2.0$ mm.

The computations were carried out using the finite element program ABAQUS (Abaqus 2016). The chosen model dimensions and the mesh fineness were chosen such that sufficient accuracy of the calculation results was ensured.

3.2 Results

Fig. 10 shows interaction diagrams derived for the considered pile (D = 2 m, L = 50 m) once in "Sand 1" and once in "Sand 2". Although the compaction behaviour in the cyclic DSS tests was quite similar for these soils (cf. Section 2), differences in the interaction diagrams are clearly recognisable. For instance, for two-way loading with $X_{mean} = 0$, the cyclic load leading to failure after 10^3 cycles is once $X_{cyc} = 0.17$ ("Sand 1) and once $X_{cyc} = 0.20$ ("Sand 2"). These results indicate a great sensitivity of the cyclic degradation behaviour to the soil's compaction behaviour and thus to the soil type.

It should be noted that the CDM method of course requires validation by comparison to model and field tests. The interaction diagrams derived here predict much greater degradations than the interaction diagram of Jardine & Standing (2012) depicted in Fig. 1. However, Puech (2013) reported an interaction diagram derived from field tests with bored piles in sand which also predicts much smaller failure load combinations for $N=10^3$ than the Jardine & Standing diagram (see also Puech & Garnier, 2017). Since in the CDM the effect of pile installation is not taken into account ("wished-in-place" procedure), the results could be considered as more representative for a bored pile. Anyway, the quantitative accuracy of the CDM surely needs further investigations.

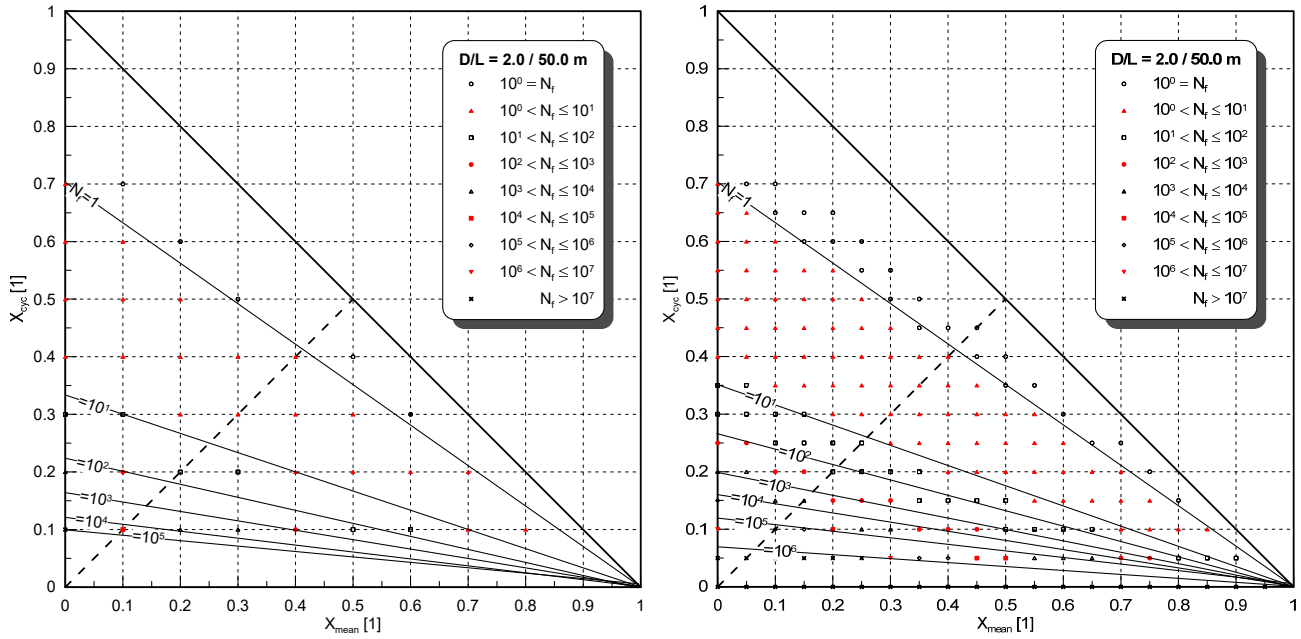

Fig. 10. Derived interaction diagrams for pile dimensions D = 2.0 m and L = 50.0 m in "Sand 1" (left) and "Sand 2" (right) at a relative density of D_r = 0.76.

4 Conclusions and outlook

The compaction behaviour of different sand soils under cyclic shear loading was examined in direct simple shear tests and the resulting effect of sand type on the capacity degradation of cyclic axially loaded piles was investigated here. The following main conclusions can be drawn:

- Different sand types – although having similar grain size distributions – show different compaction behaviour under action of cyclic shear strains. The results for the medium sands investigated indicate that the uniformity index has a greater effect than the mean grain diameter. In comparison to a medium to coarse sand examined by Silver & Seed (1971), greater volume strains were observed. Also, a significant effect of normal stress on the compaction behaviour was observed, with smaller volume strains for greater normal stresses. Contradicting the assumption of Silver & Seed (1971), it is recommended not to neglect this effect.
- In the strain-controlled tests conducted, no significant effect of the mean shear strain was observed. The volume strains only depend on the cyclic shear strain span or the cyclic shear strain amplitude, respectively.
- Application of the measured compaction behaviour in the calculation of cyclic pile behaviour with the Capacity Degradation Method (CDM) show clearly recognisable differences in the interaction diagrams derived for different sands. This is an indication for a significant sensitivity of the pile behaviour under cyclic axial loading to the sand type, i.e. grain size distribution.

Additional cyclic DSS tests with other soil types are desirable to get a deeper insight into the effects of grain size distributions and also grain shape on the compaction behaviour under cyclic shearing. Furthermore, it is intended to validate and further develop the Capacity Degradation Method (CDM) in order to investigate both pile and soil type effects on the capacity degradation of cyclic axially loaded piles.

References

ABAQUS User Manual, 2016, Simulia, Providence, RI, USA.

Achmus, M., Abdel-Rahman, K., Schäfer, D., Kuo, Y.-S., Chung, C.-Y., Tseng, Y.-H. 2017. Interaction Diagrams for Driven Steel Piles under Cyclic Axial Loading. 27th Int. Ocean and Polar Engineering Conference (ISOPE), San Francisco/USA, June 25-30.

Achmus, M., Lemke, K., Abdel-Rahman, K., Kuo, Y.-S., 2015. Numerical Approach for the Derivation of Interaction Diagrams for Piles under Cyclic Axial Loading, in: Proceedings of the 25th International Offshore and Polar Engineering Conference. pp. 755-760.

Jardine, R.J., Standing, J.R. (2012). Field axial cyclic loading experiments on piles driven in sand. Soils and Foundations, Vol. 52, No.4: 723-736.

Kirsch, F., Richter, T. & Mittag, J. (2011). Zur Verwendung von Interaktionsdiagrammen beim Nachweis axial-zyklisch belasteter Pfähle, Bautechnik 88, Heft 5, 2011 (in German).

Poulos, H.G. (1988). Cyclic Stability Diagram for axially loaded piles, ASCE Journal of Geotechnical Engineering Vol. 114, No. 8.

Puech, A. (2013). Advances in axial cyclic pile design: contribution of the Solcyp project, Proceedings TC 209 Workshop, 18th ICSMGE, Paris/ France.

Puech, A., Garnier, J. (2017). Design of Piles Under Cyclic Loading – Solcyp Recommendations, Wiley & Sons, Hoboken/ USA.

Silver, M.L., Seed, H.B., 1971. Volume changes in sands during cyclic loading. Journal of the Soil Mechanics and Foundations Division, Proceedings of the American Society of Civil Engineers, SM 9, 1171-1182.

Vucetic, M., 1994. Cyclic Treshold Shear Strains in Soils. Journal of Geotechnical Engineering, 120 (12), 2208-2228.